8942–8954 *Nucleic Acids Research, 2015, Vol. 43, No. 18* *Published online 17 September 2015*
doi: 10.1093/nar/gkv916

The *Bacteroides sp. 3_1_23* Pif1 protein is a multifunctional helicase

Na-Nv Liu[1,†], Xiao-Lei Duan[1,†], Xia Ai[1], Yan-Tao Yang[1], Ming Li[2], Shuo-Xing Dou[2], Stephane Rety[3], Eric Deprez[4] and Xu-Guang Xi[1,4,*]

[1]College of Life Sciences, Northwest A&F University, Yangling, Shaanxi 712100, China, [2]CAS Key Laboratory of Soft Matter Physics, International Associated Laboratory of CNRS-Institute of Physics, Chinese Academy of Sciences, Beijing 100190, China, [3]Institut de Biochimie et Chimie des protéines, CNRS UMR5086, 7 passage du Vercors, 69367 Lyon Cedex 07, France and [4]Laboratoire de Biologie et Pharmacologie Appliquée, ENS Cachan, CNRS UMR8113, IDA FR3242, F-94235 Cachan, France

Received February 17, 2015; Revised September 3, 2015; Accepted September 4, 2015

ABSTRACT

ScPif1 DNA helicase is the prototypical member of a 5′-to-3′ helicase superfamily conserved from bacteria to human and plays various roles in the maintenance of genomic homeostasis. While many studies have been performed with eukaryotic Pif1 helicases, including yeast and human Pif1 proteins, the potential functions and biochemical properties of prokaryotic Pif1 helicases remain largely unknown. Here, we report the expression, purification and biochemical analysis of Pif1 helicase from *Bacteroides sp. 3_1_23* (BsPif1). BsPif1 binds to a large panel of DNA substrates and, in particular, efficiently unwinds partial duplex DNAs with 5′-overhang, fork-like substrates, D-loop and flap-like substrates, suggesting that BsPif1 may act at stalled DNA replication forks and enhance Okazaki fragment maturation. Like its eukaryotic homologues, BsPif1 resolves R-loop structures and unwinds DNA–RNA hybrids. Furthermore, BsPif1 efficiently unfolds G-quadruplexes and disrupts nucleoprotein complexes. Altogether, these results highlight that prokaryotic Pif1 helicases may resolve common issues that arise during DNA transactions. Interestingly, we found that BsPif1 is different from yeast Pif1, but resembles more human Pif1 with regard to substrate specificity, helicase activity and mode of action. These findings are discussed in the context of the possible functions of prokaryotic Pif1 helicases *in vivo*.

INTRODUCTION

Helicases are adenosine triphosphate (ATP) hydrolysis-driven molecular motors that translocate unidirectionally along DNA phosphodiester backbone to separate stable DNA duplexes into single strands (1). They are essential for all nucleic acid metabolic transactions in living organisms to ensure a faithful transmission of the genetic information (1,2). The fundamental importance of helicases is highlighted by the fact that defects in helicase functions lead to human diseases characterized by genome instability and varieties of cancers (3).

Pif1 helicases are widely found in eukaryotes from yeast to human (4,5). ScPif1, as a prototypical member of the Pif1 family, is a 5′-to-3′-directed DNA helicase family and belongs to the superfamily 1 (SF1) of helicases.This protein was originally discovered by a genetic screen for mutations that affected mitochondrial DNA stability (6). Further studies have shown that Pif1 has wider roles than previously suggested. So far, the knowledge of the essential functions of Pif1 mainly comes from yeast genetic studies and biochemical characterizations of both yeast and human Pif1. The main functions of Pif1 family helicases can be summarized as: (i) Pif1 helicases maintain and stabilize mitochondrial (mt) DNA. In *Saccharomyces cerevisiae*, Pif1 (ScPif1) is associated throughout the mtDNA genome, suggesting that it prevents and/or is involved in DNA double-strand breaks (DSBs) repair at the mtDNA level or is part of the mitochondrial replisome (7–9). (ii) They negatively regulate telomere length by displacing telomerase from DNA end. Cellular and biochemical studies have revealed that ScPif1 displaces telomerase (Est2p) from the telomere end by its helicase activity (7). Interestingly, overexpression of heterologous human Pif1 protein (hPif1) in *pif1*Δ yeast strains prevents telomere lengthening and is nearly as effective as its yeast counterpart (8), suggesting that this negative regulation mechanism is conserved from yeast to human. This activity appears also necessary to prevent telomeric repeat addition at the end of DSBs (7). (iii) Besides the displacement of telomerase from the telomere end, ge-

*To whom correspondence should be addressed. Tel: +33 01 4740 7754; Fax: +33 01 4740 7754; Email: xxi01@ens-cachan.fr
†These authors contributed equally to the paper as first authors.

netic studies suggest that the second Pif1 protein in yeast, ScRrm3P, may be able to disrupt stable non-nucleosomal protein–DNA complexes at the sites where replication forks pause (9,10). Thus, Rrm3p may help to resolve 'collisions' between transcription and replication processes through its disruption activity of protein–DNA/RNA complexes (11). (iv) Pif1 helicases unfold G-quadruplex (G4) structures and prevent replication-fork stalling at G-quadruplexes. Genetic studies have established that failure of untangling G4 in Pif1-deficient cells impedes DNA transactions and leads to replication-fork impairment, unusual epigenetic silencing and significant chromosomal rearrangements (8). Among the various helicases having the ability to resolve G4 structures, it was previously shown that ScPif1 possesses a particularly high G4-unwinding activity, at least *in vitro* (12). (v) Pif1 helicases enhance the maturation of Okazaki fragments. In eukaryotic systems, Okazaki fragments are initiated by DNA polymerase α/primase (pol α) (13) followed by the action of DNA polymerase δ which, at the 5′-end of the downstream Okazaki fragment, displaces the end into a flap. Genetic evidences have suggested that Pif1 influences the flap processing by lengthening displaced flaps (14).

Although eukaryotic Pif1 helicases play multiple roles in nuclei and mitochondria, with several of them that appear to be specific to eukaryotic organisms, Pif1 helicases are also widely found in various prokaryotes (15) and comparative sequence analysis shows that the essential domains and motifs for performing helicase activity are highly conserved between eukaryote and prokaryote helicase families (15), raising the question of the possible physiological roles of prokaryotic Pif1 helicases. To date, no extensive biochemical characterization in terms of enzymatic activity and DNA substrate specificity of a prokaryote Pif1 family member has been performed, although the ability of prokaryotic Pif1 helicases to unwind G4-DNA structures has been recently reported (12).

To gain insight into the possible functions of prokaryotic Pif1 helicases, we expressed and purified the full-length Pif1 protein from *Bacteroides sp. 3_1_23* (BsPif1) and characterized its DNA-binding and unwinding properties using a wide range of possible physiological DNA substrates. We demonstrate that the recombinant BsPif1 protein binds to a wide range of DNA substrates and displays efficient unwinding activities with a large variety of DNA substrates involved in DNA replication, repair and recombination. Interestingly, from many aspects, BsPif1 is different from yeast Pif1, but qualitatively resembles human Pif1 with regard to substrate specificity, helicase activity and mode of action.

MATERIALS AND METHODS

Reagents, buffers

All chemicals were reagent grade and all buffers were prepared using high quality deionized water from a Milli-Q ultrapure water purification system (Millipore) having resistivity greater than 18.2 MΩ.cm and further filtered with a 0.20-μm filter before use. All chemicals were purchased from Sigma unless otherwise indicated.

Oligonucleotide substrates

The DNA substrates used in unwinding and DNA-binding assays as well as in dynamic light scattering (DLS) experiments were purchased from Shanghai Sangon Biological Engineering Technology & Services Co., Ltd (Shanghai, China). The structures, sequences of unlabeled or fluorescently labeled DNA substrates are shown in Supplementary Table S1. The protein trap used for single-turnover kinetic experiments was a 56-nt poly(dT), dT_{56}. All synthetic oligonucleotides were purified using denaturing polyacrylamide gel electrophoresis before storage in buffer D (10 mM Tris–HCl, pH 8.0, 1 mM EDTA) at −20°C. Concentrations of single-stranded oligonucleotides were determined spectrophotometrically based on extinction coefficients calculated by the nearest neighbor method. A 2 μM working stock of duplex or G4 DNA was prepared by mixing equimolar concentrations of complementary single-stranded oligonucleotides in a 20 mM Tris–HCl buffer (pH 7.5) containing 100 mM KCl. After heating the mixture to 95°C for 5 min, oligonucleotides were annealed by slow cooling to room temperature. The various duplex and G4 DNA substrates were stored at −20°C.

Protein expression and purification

The gene encoding BsPif1 protein (Genebank number: WP_008647876.1) was amplified with genomic DNA prepared from *Bacteroides sp. 3_1_23* strain. The amplified polymerase chain reaction (PCR) products were cloned into pET15b-SUMO (Invitrogen) using ExTaq PCR (Takara) according to the manufacturer's protocol. In this system, BsPif1 was tagged with an N-terminal Sumo fusion domain preceded by a 6x-His tag. All constructs were verified using PCR screening and sequencing (Invitrogen, Shanghai).

The BsPif1 expression vector was transformed into the *Escherichia coli* strain BL21(DE3) and cultures were performed at 37°C until an OD_{600} of ∼0.6 and then incubated overnight with 0.4 mM IPTG at 18°C. After centrifugation, the cell pellets were re-suspended in lysis buffer (20 mM Tris–HCl pH 8.0, 500 mM NaCl, 10 mM Imidazole and 10% glycerol (v/v)). The cells were sonicated and then centrifuged at 12 000 rpm for 40 min. Before loading on a Ni^{2+} charged IMAC column (GE Healthcare), the samples were filtered through a 0.45-μm filter. The protein was then eluted from the Ni^{2+} affinity column by running a 20–300 mM imidazole gradient in a 20 mM Tris–HCl buffer (pH 8.0), 500 mM NaCl and 10% glycerol (v/v). The eluted protein was incubated with Sumo protease (Invitrogen, Beijing) for 20h at 4°C and dialyzed against the lysis buffer at 4°C overnight. Then the Sumo-digested proteins were loaded on a Ni^{2+} affinity column (equilibrated in the lysis buffer) and flow through. The protein was dialyzed against buffer Q (20 mM Tris–HCl, pH 7.4, 200 mM NaCl, 1 mM EDTA, 1 mM Dithiothreitol (DTT) and 5% glycerol (v/v)), and loaded on a Source Q column (GE Healthcare). The protein was then eluted by a NaCl gradient (200–1000 mM in buffer Q). The eluted fraction containing BsPif1 was collected, concentrated and was further purified by gel filtration using a Superdex 200 10/300 GL column. The final purified protein was dialyzed against the storage buffer (20 mM Tris–HCl,

pH 7.4, 350 mM NaCl, 1 mM DTT and 20% glycerol (v/v)) and was stored at −80°C.

To produce an ATPase activity deficient mutant, the conserved glutamic acid at position 106 in the ATP hydrolysis motif II (DEIS) was mutated to alanine, resulting in the BsPif1^{E106A} mutant. The point mutation was constructed using recombinant PCR, with the desired mutations introduced in the internal mutagenic primers (Forward E106A: 5′-ctgctgattattgatgcgattagcatggtgcgc and Reverse E106A: 5′-gcgcaccatgctaatcgcatcaataatcagcag). To ensure that only the desired mutation was introduced, the PCR portions were sequenced. The procedure for expression and purification of the BsPif1^{E106A} mutant was the same as the wild-type protein. After purification, the purity of wt or BsPif1^{E106A} protein was ≥95% as judged by sodium dodecyl sulphate-polyacrylamide gel electrophoresis (SDS-PAGE) (Supplementary Figure S1). The *E. coli trp* repressor was overexpressed and purified according to Czernik at *al*. (16).

Determination of the BsPif1 molecular weight: dynamic light scattering (DLS)

DLS measurements were performed at 25°C using a DynaPro NanoStar instrument (Wyatt Technology Corporation, USA) equipped with a thermostated cell holder (17). All solutions were filtered using 0.1 μm-filters. The protein concentration was 2.0–8.0 μM in DLS buffer (50 mM Tris–HCl pH 7.5, 100 mM NaCl, 1 mM DTT) (total volume, 30 μl). The scattered light was collected at an angle of 90°. Recording times were typically in the 3–5 min range (18–30 cycles in average of 10 s each). The analysis was performed with the Dynamics 7.0 software using regularization methods (Wyatt Technology Corporation, USA). The resulting diffusion coefficient (D) was used for the calculation of the hydrodynamic (Stoke) radius (R_h) using the relationship: $D = kT/6\pi\eta_0 R_h$, where k is the Boltzmann-constant, T the temperature and η_0 the solvent viscosity. The molecular weight, M_w, was calculated from the hydrodynamic radius using the empirical Equation (1):

$$M_W(\text{kDa}) = (1.68 \times R_h)^{2.34} \quad (1)$$

Determination of the BsPif1 molecular weight: size exclusion chromatography

Size exclusion chromatography was performed at 25°C, using an FPLC system (GE healthcare), on a Superdex 200 (analytical grade) column equilibrated with buffer S (20 mM Tris–HCl, pH 7.4, 500 mM NaCl, 1mM EDTA, 1 mM DTT and 5% glycerol (v/v)). Elution was performed using the same buffer. A total of 20 μl of 2–6 μM BsPif1 was loaded on the column and was eluted at a flow rate of 0.4 ml/min in buffer S, and absorbances were monitored at 280 and 260 nm. It is well known that proteins migrate through a gel filtration column as a function of both the molecular weight and the molecular shape. The R_h value characterizing BsPif1 was determined from the plot of log R_S versus K_{av} using the different Stokes radii of the standards. The partition coefficient K_{av} was calculated using the formula: $K_{av} = (V_e - V_0)/(V_t - V_0)$, where V_e is the elution volume of the sample, V_0 is the excluded volume of the column, and V_t is the total volume of the column. The excluded volume, V_0 (7.52 ml), and the total volume, V_t (23.5 ml) were measured by calibration with dextran blue and thymidine. The calibration plot of log R_S versus K_{av} was constructed using a high and low molecular weight calibration kit from Sigma: cytochrome c (12.4 kDa; R_h = 12 Å), carbonic anhydrase (29 kDa; R_h = 22.5 Å), albumin (67 kDa; R_h = 35.5 Å), phosphorylase b (97.4 kDa; R_h = 38.75 Å) and thyroglobulin (669 kDa; R_h = 85 Å). Assuming similar shape factors, the calibration plot allowed the determination in a first approximation of the molecular weight of BsPif1.

Equilibrium DNA-binding assay

The binding of BsPif1 to fluorescein-labeled DNA substrates was analyzed by fluorescence polarization assay using Infinite F200 instrument (TECAN). Varying amounts of protein were added to a 150 μl solution of buffer A (25 mM Tris–HCl, pH 7.5, 50 mM NaCl, 2 mM $MgCl_2$ and 2 mM DTT) containing 5 nM fluorescein-labeled DNA. Each sample was allowed to equilibrate in solution for 5 min. After 5 min, the steady-state fluorescence anisotropy (r) was measured. A second reading was taken after 10 min, in order to ensure that the mixture was well-equilibrated and stable. Less than 5% change was observed between the 5- and 10-min measurements. The equilibrium dissociation constant was determined by fitting the binding curves using Equation (2):

$$\Delta r = \Delta r_{max} \times P/(K_d + P) \quad (2)$$

where Δr_{max} is the maximal amplitude of the anisotropy ($= r_{max,complex} - r_{free\ DNA}$), P is the helicase concentration and K_d is the midpoint of the curve corresponding to the apparent dissociation constant.

Stopped-flow FRET measurements

We used a stopped-flow FRET assay (18) for measuring unwinding kinetic rate constants of BsPif1, using doubly labeled DNA substrates, with fluorescein and hexachlorofluorescein as a donor and acceptor, respectively. The stopped-flow FRET assay was carried out using a Bio-Logic SFM-400 mixer with a 1.5 × 1.5 mm cell (FC-15, Bio-Logic, France) and the Bio-Logic MOS450/AF-CD optical system equipped with a 150-watt mercury-xenon lamp (18). Fluorescein was excited at 492 nm (2-nm slit width) and its emission was monitored at 525 nm using a high pass filter with 20-nm bandwidth (D525/20; Chroma Technology Co.). Unwinding kinetics were measured in a two-syringe mode, where BsPif1 helicase and DNA substrates were pre-incubated in the unwinding reaction buffer A (25 mM Tris–HCl pH 7.5, 50 mM NaCl, 2 mM $MgCl_2$ and 2 mM DTT) at 25°C for 5 min (in syringe 3) and the unwinding reaction was initiated by rapid mixing with ATP +/− protein trap (in syringe 4). All reported concentrations correspond to final concentrations, i.e. after mixing. For converting the output voltage to a percentage of unwinding, a calibration experiment was performed in a four-syringe mode, with helicase in syringe 1, hexachlorofluorescein-labeled and fluorescein-labeled single-stranded oligonucleotides in syringe 2 and 3, respectively, and ATP +/− protein trap in syringe 4. The

fluorescent signal of the mixed solution from the four syringes corresponded to 100% unwinding. All of the solutions were filtered and extensively degassed just before use. The stopped-flow temperature was controlled by an external thermostated water bath (Ministat 125; Huber) and a high flux pump. The standard reaction was performed with 4 nM DNA substrates, 3 mM ATP and 100 nM BsPif1 in buffer A.

Kinetic Data Analysis: all stopped flow kinetic traces were an average of over 10 individual traces. The kinetic traces were analyzed using Bio-Kine (version 4.26; Bio-Logic, France). To determine the step-size with the n-step sequential model (19), the single-turnover unwinding data curves were fitted using Equation (3):

$$A(t) = A\left[1 - \sum_{r=1}^{n} \frac{k_{\text{obs}}^{r-1} t^{r-1}}{(r-1)!} e^{-k_{\text{obs}} t}\right] \quad (3)$$

where $A(t)$ represents the unwinding amplitude as a function of time, A is the total unwinding amplitude and k_{obs} is the apparent unwinding rate constant. n is the number of steps required to unwind the duplex DNA. After each purification, some standard reactions, such as unwinding of duplex DNA and G4 substrates, were carried out and unwinding activities were found to be reproducible (no significant difference was observed between preparations).

ATPase assay

DNA-dependent ATPase activity was measured using a commercial ATPase assay kit according to manufacturer's instructions (Innova Biosciences). See more details in Supplementary Materials and Methods.

RESULTS

General structural and biochemical properties of purified BsPif1

The apparent molecular weights of the wt-BsPif1 and the BsPif1^{E106A} ($M_W \approx 50$ kDa), as determined by SDS-PAGE, were consistent with the theoretical M_W (Supplementary Figure S1). To determine the oligomeric state of BsPif1 in solution, we first analyzed its elution profile in size-exclusion chromatography column. In the 2–8 μM concentration range, BsPif1 elutes as a single peak ($K_{av} = 0.4$), which corresponds to an apparent M_W of 48–50 kDa (Figure 1A), suggesting that BsPif1 is monomeric in solution. The oligomeric status of BsPif1 in solution was further confirmed by DLS in the same protein concentration range. The hydrodynamic radius of apo-BsPif1 was 3.17 nm (Table 1), in agreement with a 47 kDa-protein, assuming a conventional degree of hydration (0.4–0.5 g H_2O/g protein) or based on Equation (1) and confirming size-exclusion chromatography results.

To address whether BsPif1 ligands could induce oligomerization of Pif1, we further determined the hydrodynamic radius of BsPif1 helicase complexed with either DNA (ssDNA or G4), or ATP-γ-S, a nonhydrolyzable ATP analogue. DLS results show that the hydrodynamic radii characterizing the different complexes correspond to M_W between 49 and 55 kDa (Table 1), indicating that neither DNA (16-nt ssDNA or G4 DNA) nor ATP-γ-S significantly influenced the oligomeric status of BsPif1 which was consistently monomeric, regardless of the experimental condition. This is in sharp contrast with ScPif1 which has been shown to be monomeric in solution, but shifted toward a dimeric form upon binding to DNA (20) and may reflect intrinsic and specific properties of BsPif1 in terms of structural organization.

In order to determine experimental conditions compatible with optimal DNA unwinding activity, we next characterized the effects of pH, DTT concentration, nature of the nucleotides, divalent cations and the ratio of ATP/Mg^{2+} on the BsPif1-catalyzed unwinding rate constant and the reaction amplitude using a 26-nt over-hanged 17-bp DNA (5′Oh$_{S26D17}$; Supplementary Table S1). The unwinding rate, as determined by stopped-flow FRET experiments (21), displayed a bell-shaped response as a function of pH with an optimal response in the pH range of 7.2–8.5 (Figure 1B). The rate value was also strongly dependent on DTT concentration, with an optimum response at 2 mM (Figure 1C). We next determined whether BsPif1, like its eukaryotic homolog ScPif1, has a preference for adenosine nucleotides (ATP and dATP) as an energy source (6). The unwinding activity was then assayed in the presence of the different types of nucleotides triphosphates (NTP) and deoxynucleotide triphosphates (dNTP). Under identical experimental conditions, all nucleotides promoted helicase activity of BsPif1 in a similar manner, except for GTP or dGTP which led to 50–60% of the maximum helicase activity in terms of unwinding kinetic rate (Figure 1D). When ATP was replaced by AMP–PNP or using an ATP-hydrolysis deficient mutant BsPif1^{E106A}, no helicase activity was observed (Figure 1D). These results indicated that BsPif1 helicase can use the energy derived from the hydrolysis of a wide range of nucleotides to unwind DNA. Regarding the influence of the metallic cofactor, BsPif1 was fully and equally active for DNA unwinding in the presence of either Mg^{2+} or Mn^{2+} (Figure 1E). This activity was significantly reduced in the presence of cobalt, copper, iron, zinc, calcium or nickel (Figure 1E). Characterization of the unwinding activity as a function of the ATP/Mg^{2+} ratio indicated that the optimum ratio was ≈1.5 (Supplementary Figure S2A–C).

ATP hydrolysis activity of BsPif1 as a function of ATP concentration displayed a classical Michaelis–Menten curve with a catalytic rate constant of 1980 min^{-1} at 37°C (Figure 1F), a value which is comparable to the values of 1000 min^{-1} at 30°C and 5000 min^{-1} at 37°C for hPif1 and ScPif1, respectively (6,22). Another important parameter, which characterizes helicase family members, concerns the DNA unwinding polarity. It is defined by the backbone polarity of the flanking ssDNA that promotes unwinding initiation and defines in turn the direction of helicase movement along this strand. To determine the polarity of the BsPif1 helicase, the partial duplex DNA substrates with either 3′- or 5′- single-stranded overhang were used (3′-Oh$_{S14D16}$ and 5′-Oh$_{S14D16}$, respectively). Clearly, BsPif1 unwound the 5′-ss overhang-containing substrate only (Supplementary Figure S2D), indicating that BsPif1 is a unidirectional helicase with a 5′-3′ polarity, in accordance with all Pif1 family helicases characterized so far (23).

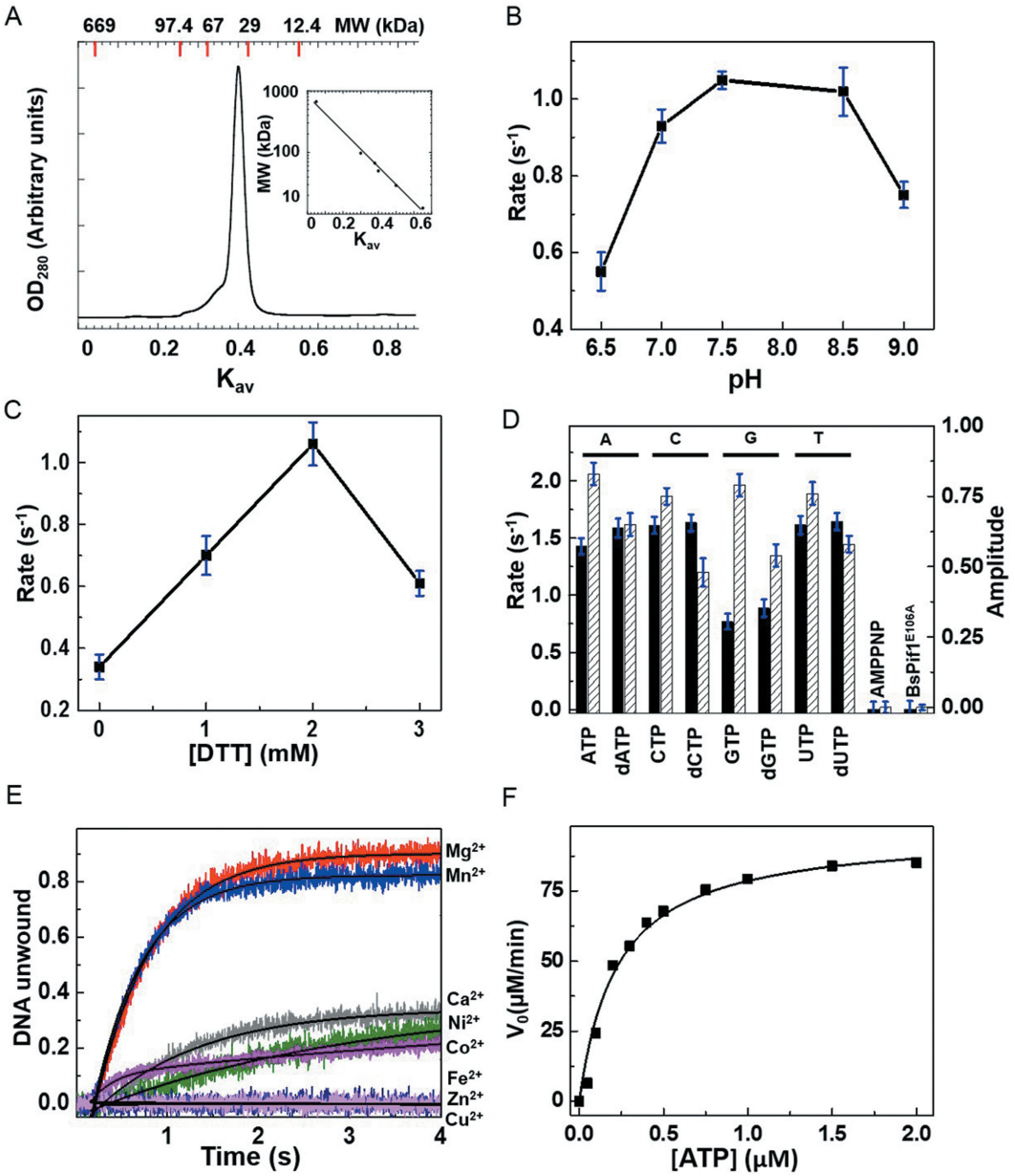

Figure 1. General biochemical properties of recombinant BsPif1. (**A**) Size-exclusion chromatography was performed as described in 'Materials and Methods' section. The elution profile corresponds to the absorbance at 280 nm. Molecular weights used for the calibration are indicated on the top axis. The insert shows the plot of standard molecular weights versus K_{av} values. The K_{av} characterizing BsPif1 (0.4) corresponds to a M_W of ∼50 kDa. Protein concentration was 3 μM (similar results were obtained using BsPif1 concentrations from 2 to 8 μM). (**B**) pH-dependent BsPif1 unwinding activity. A total of 30 mM Na-MES and Tris–HCl buffers containing 50 mM NaCl and 2 mM $MgCl_2$ were used for the pH intervals 6.0–7.0 and 7.2−9.0, respectively. ATP and DTT concentrations were 3 and 2 mM, respectively. (**C**) BsPif1 unwinding activity as a function of DTT concentration. Unwinding activity was assayed in the presence of increasing DTT concentrations in a Tris–HCl buffer (pH 7.5) containing 50 mM NaCl, 2 mM $MgCl_2$ and 3 mM ATP. (**D**) BsPif1 unwinding activity in the presence of various nucleotides (1 mM). Reactions were performed in buffer A (25 mM Tris–HCl, pH 7.5, 50 mM NaCl, 2 mM $MgCl_2$ and 2 mM DTT). The unwinding rates (solid bars) and reaction amplitudes (hatched bars) were determined as described under 'Materials and Methods' section. (**E**) Metal ion substitution for Mg^{2+} in BsPif1-catalyzed unwinding reaction. Helicase reaction was performed as explained under the standard unwinding condition using 3 mM ATP in the presence of various metal ions (2 mM). All unwinding assays in panels B–E were performed using 100 nM BsPif1 and 4 nM DNA substrate (5′-Oh_{S26D17}). (**F**) ATPase activity of BsPif1. The initial rate of ATP hydrolysis, determined as explained in Supplementary Materials and Methods using 50 nM BsPif1 in the presence of a 67-mer ss oligonucleotide (25 μg/ml), on ATP concentration. Reactions were carried out in buffer A at 37°C. Data were fitted to the Michaelis–Menten equation. V_{max} was estimated to be 99 μM·min^{-1} and k_{cat} = 1980 min^{-1} ($[BsPif1]_{TOTAL}$ = 50 nM); K_M = 0.2 μM.

Table 1. Hydrodynamic radius of BsPif1 helicase +/− DNA or +/− ATP-γ-S as determined by DLS

Substrate/ligands	Concentration	Radius (nm)	%Mass	Calculated mass (kDa)
BsPif1	3 μM	3.17 ± 0.29	99.9 ± 0.1	47 ± 2.7
+ATPγS	1 mM	3.18 ± 0.12	99.8 ± 0.2	49 ± 4.3
+ssDNA (16nt)	3 μM	3.20 ± 0.11	100 ± 0.1	51 ± 6.7
+G4 DNA	3 μM	3.30 ± 0.17	97.7 ± 2.2	55 ± 10.2

BsPif1 binds to a broad range of DNA substrates

To probe possible physiological functions of BsPif1 in cell, we first studied the DNA-binding properties using a variety of DNA substrates which resemble intermediates of DNA transactions (Figure 2A). The binding dissociation constant (K_d) for each DNA substrate was determined by steady-state fluorescence anisotropy (see 'Materials and Methods' section and Supplementary Figure S3). The determined binding site-size is about 8∼10 nt (Supplementary Figure S4) and the K_d values are summarized in Table 2. The binding affinity of BsPif1 for the different DNA substrates can be classified into three levels according to the determined K_d values (Figure 2B): (i) BsPif1 displays relatively higher binding affinities, with K_d values ranging from 20 to 40 nM, for a 'Y-structure' DNA substrate (Y-S), ssDNA (S16), a partial duplex DNA with 5′- or 3′-overhanged ssDNA (3′-Oh and 5′-Oh), three way junction DNA (TWJ), G4 and G4 with 3′- or 5′-overhanged ssDNA (substrates: G4, 3′-G4 and 5′-G4); (ii) BsPif1 binds to 5′- or 3′-flap-containing DNAs (5′-FL and 3′-FL) and bubble-containing DNA (BS4 and BS12) with intermediary K_d values, ranging from 55 to 75 nM; (iii) BsPif1 displays lower binding affinities with K_d values higher than 140 nM for blunt-ended dsDNA (D16) and Holliday junction DNA (HJ). In summary, BsPif1 formed stable protein–DNA complexes with all of the substrates tested and with the highest affinity obtained for the forked duplex DNA (Y-S) (K_d = 18.4 nM) and the lowest affinity for the blunt-end dsDNA (K_d = 232.1 nM). Interestingly, the determined K_d values for all these G4 substrates and the Y-structure DNA were comparable. This is in sharp contrast to the results obtained with ScPif1 which binds to G4 DNA 500-fold better than Y-structure (12) .

BsPif1 unwinds a broad range of DNA substrates but prefers 5′-tailed duplex DNA substrates

Different structured DNAs were labeled appropriately with fluorescent groups to determine both unwinding rate constants and reaction amplitudes by stopped-flow FRET assay (18). Among the various DNA substrates tested (results are explicitly shown in Figure 2C for eight substrates; results relative to other substrates are summarized in Table 2), a common feature for DNA structures efficiently unwound corresponds to the presence of a 5′-ss tail. This is the case for 5′-ss overhang-containing DNA substrate (5′-Oh_{S12D20}), Y-S and 5′-FL. Their substrate counterparts or other DNA structures with 3′-ss overhang or without ss overhang display no or lower activities such as 3′-FL, TWJ and HJ, BS4 and BS12 (Figure 2C and Table 2). To note, the property that BsPif1 unwinds more efficiently 5′-ss overhang duplex DNA than forked duplex DNA is again in sharp contrast to the situation of ScPif1 which is intrinsically more active for unwinding Y-structure than 5′-ss overhang duplex DNA (24), but closely resembles hPif1 from this point of view (23). Previous studies have shown that ScPif1 accelerate DNA annealing (25). We confirmed that, in our hands, ScPif1 was competent for promoting DNA annealing; however, under identical experimental conditions, BsPif1 failed to catalyze DNA annealing (Supplementary Figure S5).

Kinetic properties of BsPif1-mediated DNA unwinding

We next determined enzymatic parameters of BsPif1 such as the unwinding rate constant, step-size and processivity. To compare with kinetic properties of ScPif1, recently characterized by others (24), we used a series of 14-nt-tailed ssDNA/dsDNA substrates with varying lengths of the duplex region, from 12- to 20-bp to determine the kinetic step-size. The experiments were performed under single-turnover experimental conditions and the characteristic unwinding curves for 12-, 16- and 20-bp duplex substrates are shown in Figure 3A. The unwinding amplitude decreased and the lag phase increased when increasing the length of the duplex region, indicating that BsPif1 takes more steps to unwind long duplex DNA and is prone to dissociate before achieving complete unwinding. The kinetic parameters (unwinding rate constant, reaction amplitude, number of steps) measured with substrates having different lengths of the duplex region were determined by fitting unwinding curves using Equation (3). The plot of the number of steps required to unwind the duplex DNA against the length of the duplex region was fitted by a linear equation, yielding a slope and an x-intercept values of 1 and 4, respectively (Figure 3B). These parameters suggest that the global kinetic step-size (m) of BsPif1 is 1 and the number of base pairs spontaneously melt is 4. The step-size of BsPif1 is identical to the one previously determined with ScPif1, even though the number of base pairs spontaneously melt as determined under our experimental condition is lower (6-bp for ScPif1 reported in (24)). Furthermore, we determined the BsPif1 processivity using the following relationship: $A = A_0 \times P^{(L/m)}$, where L is the length of the duplex region, m is the step-size parameter and A_0 the initial amplitude. We found that the P value was 0.92, indicating that the average unwinding distance is about 12.5 bases (= 1/(1–P)) before dissociation from DNA. The above determined values for step size, unwinding rate constant and processivity are in good agreement with those previously determined for ScPif1 (24).

To get deeper insight into the relationship between unwinding activity and ATP concentration, we performed unwinding kinetics using 5′-Oh_{S26D17} under single-turnover conditions in the presence of varying ATP concentrations (from 0.05 to 1 mM). The unwinding reaction was initiated by addition of 5 μM dT_{56} and ATP. Typical unwinding time-courses are shown in Figure 3C. The k values, as de-

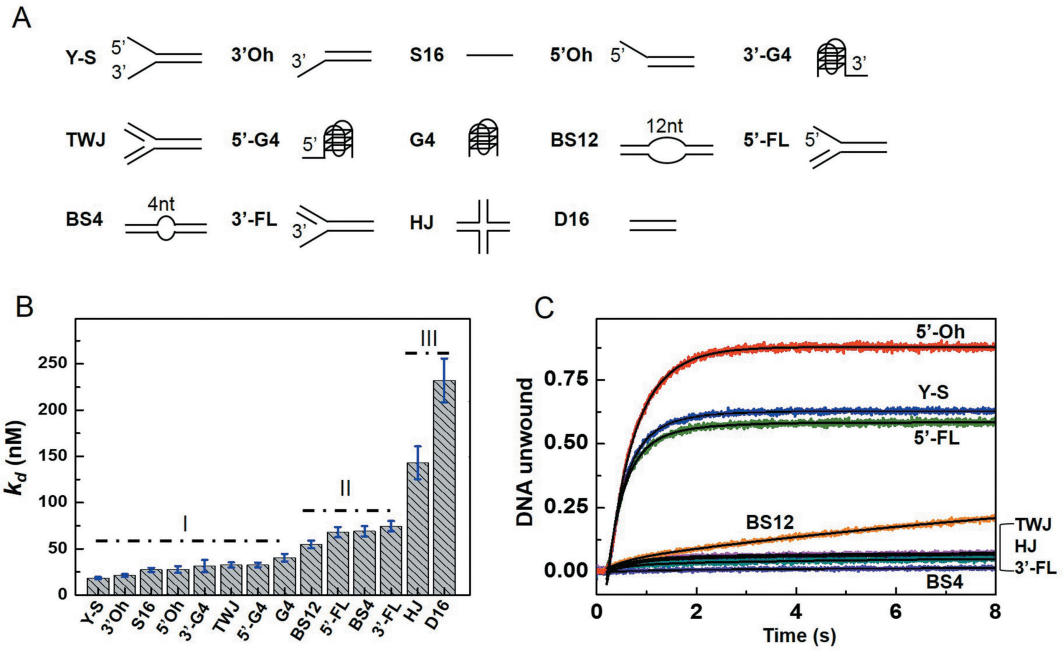

Figure 2. Binding and unwinding characteristics of BsPif1 helicase using various DNA substrates. (**A**) Schematic presentation of the DNA substrates used in the binding and unwinding experiments. (**B**) BsPif1 binds to a broad range of DNA substrates. A total of 5 nM of fluorescently labeled DNA substrate was titrated with increasing concentrations of BsPif1. The dissociation constants (K_d) were derived from the fits of experimental curves obtained at 25°C as described in 'Materials and Methods' section. Error bars indicate S.D ($n = 3$–4). Binding isotherms are shown in Supplementary Figure S3 and K_d values are summarized in Table 2. (**C**) BsPif1-catalyzed unwinding kinetics with various DNA substrates. Unwinding reactions were performed and analyzed as described in 'Materials and Methods' section. The plots shown in panel C are representative of three independent experiments.

Table 2. Binding and unwinding parameters for different substrates*

P \ S	S16	S24	S32	D16	Y-S	3'Oh_{S12D20}	5'Oh_{S12D20}	3'-FL	5'-FL	TWJ
K_d (nM)	27.4±2.2	27.6±3.1	21.4±2.6	232.1±23.7	18.4±1.2	21.3±1.5	27.8±3.6	74.5±5.5	67.9±5.6	32.5±2.8
Rate (s^{-1})					1.56±0.17	0.01±0.02	2.17±0.23	0.11±0.01	1.71±0.19	0.12±0.03
Amplitude					0.60±0.02	0.03±0.01	0.94±0.02	0.08±0.01	0.67±0.03	0.08±0.01

P \ S	HJ	BS4	BS12	3'-G4	5'-G4	G4	5'-Oh_{30}	$S_{30}D/R_{12}$	$S_{20}D/R_{12}$	$S_{20}D/R_{22}$
K_d (nM)	143.2±17.8	69.1±5.5	54.9±4.1	32.6±2.6	31.4±6.8	40.5±4.1				
Rate (s^{-1})	0.08±0.01	0.01±0.01	0.09±0.01	0.05±0.01	1.76±0.19	0.55±0.08	2.51±0.26	0.49±0.07	0.18±0.03	0.14±0.02
Amplitude	0.06±0.01	0.01±0.01	0.42±0.02	0.11±0.02	0.90±0.01	0.65±0.01	0.86±0.01	0.61±0.02	0.31±0.01	0.43±0.02

P \ S	FD/R_{12}	R-loop	5'-$Flap_{30}$-A	5'-$Flap_{30}$-B	TWJ-$Flap_{20}$-A	TWJ-$Flap_{20}$-B	D-loop
K_d (nM)							
Rate (s^{-1})	0.12±0.02	0.79±0.08	2.95±0.32	2.52±0.27	0.07±0.01	2.02±0.21	0.21±0.03
Amplitude	0.59±0.02	0.32±0.01	0.90±0.02	0.81±0.03	0.06±0.01	0.64±0.02	0.68±0.02

* The *mean values* and standard deviations were determined from 3-5 independent measurements.

S, Substrate; **P**, Parameters; 5'-$Flap_{30}$-A: downstream primer of 5'-flap was labeled; 5'-$Flap_{30}$-B: upstream primer of 5'-flap was labeled.

TWJ-$Flap_{20}$-A: downstream primer of TWJ-like DNA was labeled; TWJ-$Flap_{20}$-B: upstream primer of TWJ-like DNA was labeled

Table 3. DNA unwinding parameters of single-turnover kinetics

	5′-Oh$_{S14D12}$	5′-Oh$_{S14D16}$	5′-Oh$_{S14D20}$
Amplitude	0.61 ± 0.05	0.45 ± 0.02	0.15 ± 0.04
k_{obs} (s^{-1})	41.6 ± 0.07	43.4 ± 0.03	39.13 ± 0.04

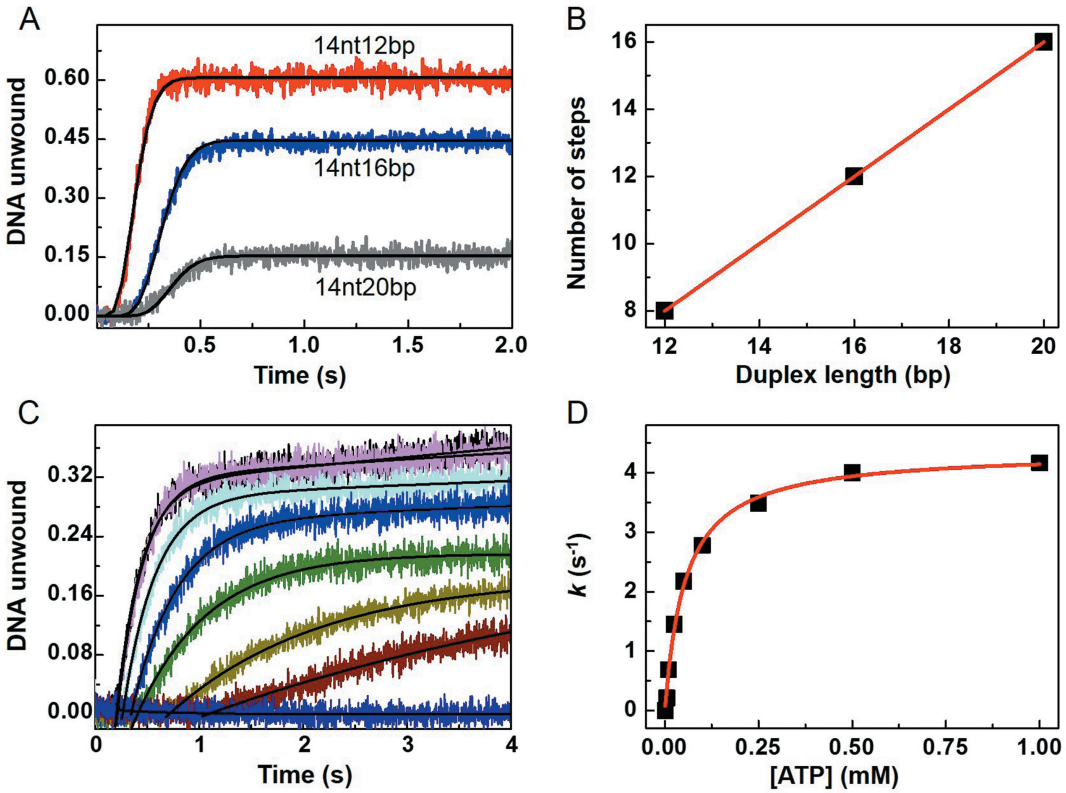

Figure 3. Single-turnover DNA unwinding reactions properties. (**A**) The experiments were performed using 4 nM of 14-nt tailed duplex DNAs with varying lengths of the duplex region (from 12- to 20-bp) (see Supplementary Table S1 for substrate sequences). The unwinding reaction was initiated by adding 3 mM ATP and 5 μM dT_{56} as protein trap at 25°C. The solid lines correspond to the best fits using Equation (3) and leading to $n = 8$, 12 and 16 for the 12-, 16- and 20-bp substrates, respectively. Fitted values corresponding to reaction amplitudes (A) and apparent kinetic rate constants (k_{obs}) are summarized in Table 3. (**B**) Number of steps required for DNA unwinding as a function of the length of the duplex region. The linear fit gives a slope of 1 (= step-size) and x-intercept of 4 (= number of bp spontaneously melt). (**C**) Single-turnover unwinding kinetics at different ATP concentrations. DNA substrate (5′ Oh$_{S26D17}$) and BsPif1 concentrations were 4 and 100 nM, respectively and the unwinding reaction was initiated with various ATP concentrations. The single-turnover unwinding rate constants, k, were fitted using a single-exponential model and are reported on the y-axis in panel **D**. (D) Plot of k as a function of ATP concentration. The best fit was obtained with a standard hyperbolic saturation function, $k = k_{max}$ [ATP/(ATP + $K_{d,ATP}$)], giving $K_{d,ATP}$ = 50.4 ± 1.7 μM. The plots in panels A and C are representative of three independent experiments.

duced from Figure 3C, were plotted against ATP concentration giving typical hyperbolic curves (Figure 3D) suggesting that BsPif1 unwinding activity does not display cooperativity on ATP concentration. Therefore, this excludes that the functional state of the active BsPif1 is a multimer (26). It also excludes an alternative explanation that BsPif1 binds cooperatively to DNA as a monomer (27). Together, the size-exclusion chromatography, DLS results and the stopped-flow experiments show that monomeric BsPif1 binds to DNA in a non-cooperative manner and probably functions as a monomer.

BsPif1 unwinds more specific structured DNA

Previous genetic and biochemical characterizations of yeast or human Pif1 showed that Pif1 enhances Okazaki fragment maturation by lengthening displaced flaps (28–31), rescues stalled replication fork (8,12) and promotes the migration of D-loop through unwinding newly-synthesized DNA strand (32,33). To study whether BsPif1, like its eukaryotic homologs, has the ability to resolve these DNA metabolic intermediates, we tested a series of DNA substrates mimicking intermediates of Okazaki fragment processing, three way junctions and D-loop DNAs. For each DNA substrate, we determined the unwinding rate constant and the corresponding reaction amplitude using the stopped-flow FRET method.

Like its human homolog, BsPif1 efficiently unwinds 5′-flap structures although BsPif1 was more efficient with the downstream primer (5′-Flap$_{30}$-A; 5′-flap primer was labeled) than the upstream primer (5′-Flap$_{30}$-B; leading strand was labeled) (2.9 s^{-1} versus 2.5 s^{-1}, respectively; Figure 4A and Table 2). However, BsPif1 was inefficient to un-

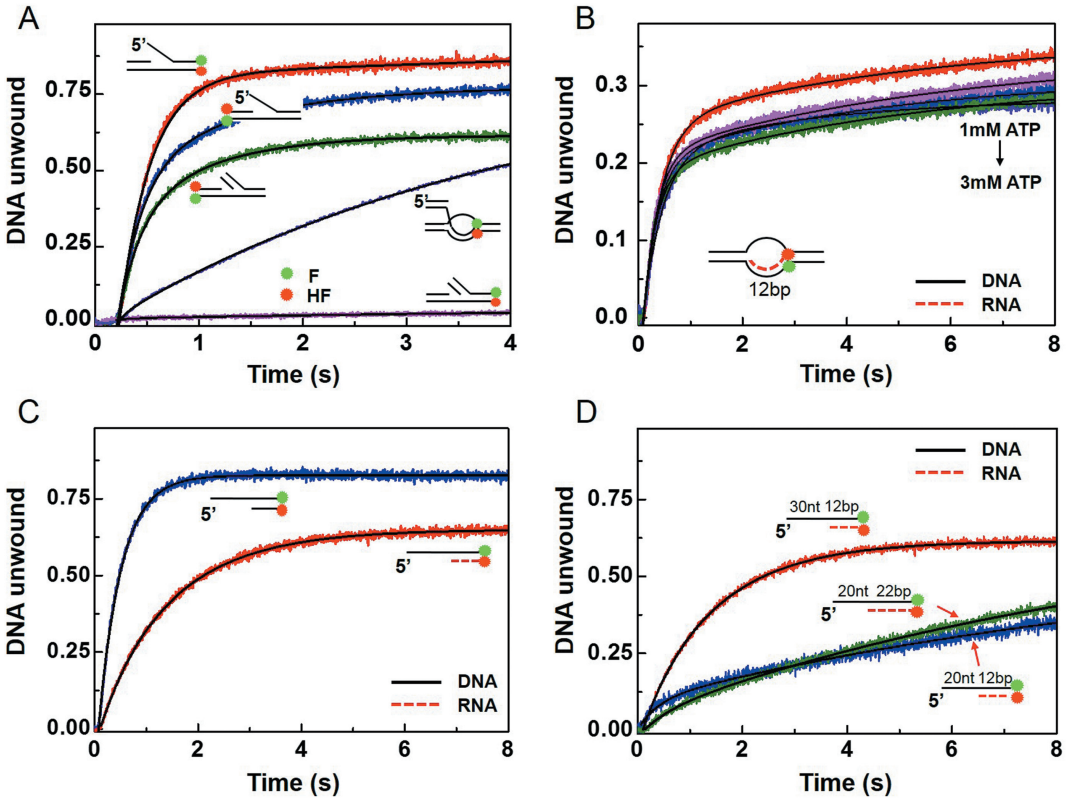

Figure 4. BsPif1 unwinds more specific structured DNA and RNA substrates. (**A**) BsPif1-mediated unwinding of flap, three way junction and D-loop DNA structures (the fluorescently labeled DNA substrates are shown in Supplementary Table S1). All curves represent the average of at least 10 individual traces and the different plots are representative of three independent experiments. The kinetic rate constants (*k*) and reaction amplitudes (*A*) are reported in Table 2. (**B**) R-loop unwinding as a function of ATP concentration (from 1 to 3 mM). *k* and *A* were 0.82 ± 0.01 s^{-1} and 0.38 ± 0.01 for 1 mM ATP and 0.79 ± 0.01 s^{-1} and 0.32 ± 0.01 for 3 mM ATP. (**C**) Unwinding of DNA–DNA (5′-Oh_{30}) and RNA–DNA ($S_{30}D/R_{12}$) substrates. (**D**) RNA–DNA unwinding as a function of the ss-tail length or the duplex region length. Fitted values of *k* and *A* are summarized in Table 2. Protein and DNA concentrations were 100 and 4 nM, respectively.

wind a TWJ-like DNA (TWJ-$Flap_{20\text{-}A}$) which corresponds to a branched molecule having three duplex arms, mimicking a stalled replication fork with double-stranded leading and lagging strands (Figure 4A). Interestingly, when the pair of fluorophores was labeled on opposite positions (TWJ-$Flap_{\mathbf{20\text{-}B}}$), allowing the measurement of the leading strand unwinding (Figure 4A), we found a significantly higher unwinding activity of BsPif1 (2 s^{-1}; reaction amplitude of 64%). These properties relative to the unwinding of the TWJ substrate by BsPif1 are comparable with hPif1, for which the unwinding of the fragment associated with the lagging strand was undetectable while the reaction amplitude relative to the leading strand was 60–65%, as deduced from gel-shift assay (23). BsPif1 activity was also tested on a DNA substrate mimicking a D-loop. The D-loop structure was originally discovered in mammalian mitochondrial DNA (34). As shown in Figure 4A, BsPif1 significantly unwinds the D-loop with an unwinding rate constant of 0.21 ± 0.01 s^{-1} and a reaction amplitude of 68% (Table 2).

BsPif1 unwinds R-loop and DNA/RNA duplexes

An R-loop is formed on a duplex DNA when a RNA sequence is stably base-paired with one of the DNA strands, resulting in displacement of the other DNA strand as a single-stranded loop. Although R-loop corresponds to key intermediates which are involved in specific cellular processes, its accumulation in cells may influence gene expression and is a potential source of genome instability (35). The ability of BsPif1 to unwind R-loop was tested using a substrate formed by the hybridization of a hexachlorofluorescein-labeled RNA with a fluorescein-labeled DNA (Figure 4B). We found that BsPif1 sustained a significant activity of R-loop unwinding with an unwinding rate constant of 0.79 s^{-1}. This unwinding activity was nearly constant in the 1–3 mM ATP concentration range (Figure 4B).

It was previously reported that ScPif1 unwinds more efficiently the RNA/DNA substrate than the DNA/DNA duplex (36). To evaluate whether BsPif1 displays similar features, the unwinding activity of BsPif1 on DNA/DNA and DNA/RNA duplexes was studied using substrates having the same length for both ss and ds regions and the same nucleotide sequence. We found that, in contrast to ScPif1, BsPif1 was more potent for unwinding the DNA/DNA substrate than the RNA/DNA substrate both in terms of unwinding rate constants (2.5 s^{-1} versus 0.5 s^{-1}) and reaction amplitudes (86 versus 61%) (Figure 4C). We also found that the 5′-ssDNA overhang length significantly influences the RNA/DNA unwinding activity. When the ss-

DNA length was increased from 20 to 30 nt (substrates $S_{20}D/R_{12}$ and $S_{30}D/R_{12}$; Supplementary Table S2), both the unwinding rate constant and the reaction amplitude of BsPif1-mediated RNA/DNA unwinding increased (2.72- and 1.97-fold changes, respectively)(Figure 4D). However, the duplex length is less critical as we observed that for a given ssDNA length (e.g. 20-nt), BsPif1 unwound 12- and 22-bp DNA/RNA duplexes (substrates $S_{20}D/R_{12}$ and $S_{20}D/R_{22}$) with similar unwinding rates and amplitudes (Figure 4D). This is different from the behavior observed with DNA/DNA duplexes where both parameters rapidly decreased as the duplex length increased (compare Figures 3A and 4D).

Unwinding of G-quadruplexes (G4) by BsPif1

To evaluate quantitatively BsPif1-mediated G4 unwinding activity, we designed a G4 substrate mimicking the stalled replication fork by G4-DNA in which the G4 motif was linked to a ssDNA at its 5′ end and to a duplex region at the 3′-end (5′- $S_{26}G4_{D17}$) (Figure 5A (insert)). Such a design allowed the monitoring of G4 unwinding in real time using the stopped-flow FRET assay (21). First, we checked that the assay actually accounts for the proper BsPif1-dependent G4 unwinding reaction, but not for the duplex region unwinding (Supplementary Figure S6). We then compared the catalytic parameters for BsPif1-dependent unwinding of G4 structures and the partial duplex DNA unwinding by using a partial duplex DNA which contains or not a G4 motif insertion at the ss/dsDNA junction (Figure 5A). BsPif1-dependent unwinding of the two DNA structures were comparable in terms of reaction amplitude (90%) with, however, a higher kinetic rate constant for 5′-$S_{26}D_{17}$ (2.9 s^{-1}) than 5′- $S_{26}G4_{D17}$ (1.8 s^{-1}) (Figure 5A). To note, without ssDNA tail or with a tail at the 3′-end, lower or no G4 unwinding activity was observed (Table 2). Moreover, no G4 unwinding activity was observed with the ATPase deficient mutant ($BsPif1^{E106A}$), indicating that G4 unwinding by BsPif1 is actually ATP-dependent and that G4 cannot be unwound through an alternative mechanism corresponding to an equilibrium displacement from a transient unfolded G4 structure toward a ssDNA form. The BsPif1-dependent G4 unwinding was next studied as a function of ATP concentration under single turnover experimental conditions. The curve was well-fitted with a hyperbolic saturation function (Hill coefficient of 1) (Figure 5B), suggesting that BsPif1 unwinds G4 structures as a monomer.

Disruption of nucleoprotein complex

The *trp* repressor serves as a model system to address the ability of helicases to displace DNA-binding proteins (37). The binding of *E. coli trp* repressor to the TrpEDCBA operator sequence was well-characterized and it has been shown that this interaction is characterized by a high affinity ($K_d = 3.2\times10^{-10}$ M) in the presence of L-Trp (38). We further confirmed that 0.5 mM L-Trp is optimum under our experimental condition (Supplementary Figure S7) according to a previous study (37). To evaluate whether BsPif1 is competent for disrupting a nucleoprotein complex, we designed an experiment in which the kinetic of BsPif1-dependent *E. coli trp* repressor displacement from dsDNA is monitored using the stopped-flow methodology, either by measuring FRET (Supplementary Figure S8) as mentioned above or using fluorescence enhancement of a single fluorophore (Figure 5C and D). By determining the BsPif1-mediated unwinding of a ss/ds DNA substrate (Supplementary Table S2) in the presence or absence of 100 nM *trp* repressor protein, we found that the time course of DNA unwinding was not influenced by the presence of *trp* repressor in terms of both unwinding rate constants and reaction amplitudes (Supplementary Figure S8), suggesting that BsPif1 could efficiently displace the *trp* repressor from the TrpEDCBA operator, concomitant to DNA unwinding.

To gain further insight into the mechanism of BsPif1-mediated nucleoprotein disruption, we designed an experiment in which the kinetics of BsPif1-mediated translocation and unwinding activities were measured in the presence or absence of the *trp* repressor using a hexachlorofluorescein-labeled DNA substrate (Figure 5C). This substrate consists of a 16-bp partial duplex containing a TrpEDCBA operator sequence with a 22 polyT at its 5′-end and labeled with hexachlorofluorescein at the ss/dsDNA junction (Trp-D16-HF, Supplementary Table S2). First, the binding of BsPif1 alone led to a modest fluorescence enhancement (from 0.72 to 0.74; green line in Figure 5C); the subsequent binding of *trp* repressor resulted in a much more significant fluorescence enhancement (from 0.74 to 1.2; purple line). Upon addition of 1 mM ATP, the fluorescence signal further increased and then decreased in both situations, i.e. BsPif1 alone or BsPif1 + *trp* repressor (Figure 5C, blue and red lines, respectively). The increasing and decreasing phases correspond to the BsPif1 translocation from the 5′-ssDNA tail to the ss/dsDNA junction and the proper DNA unwinding of the duplex region, respectively. In the presence of protein trap, as shown in Figure 5C, BsPif1 did not disrupt *trp* repressor from TrpEDCBA operator, since the final fluorescence signal value corresponded to the value characterizing the DNA-bound form of *trp* repressor, suggesting a post-catalytic *trp* repressor re-binding to DNA. However, in the absence of protein trap, allowing multiple turnovers of BsPif1 or, alternatively, the concerted action of multiple proteins on the same substrate, the result was clearly different; after the increasing phase, the amplitude of the decreasing phase was much larger with a final value of fluorescence intensity corresponding to *trp* repressor-free DNA (Figure 5D). To note, the final values also indicate that BsPif1 did not dissociate from DNA when it reached the DNA 3′-end, regardless of the condition, single or multiple turnover, with probably one protein which remains associated with the DNA 3′-end in both conditions. Our results indicate that in the latter case (multiple turnover condition), BsPif1 efficiently displaced the *trp* repressor from the TrpEDCBA operator concomitantly to unwinding. This BsPif1-dependent protein disruption property is similar to the previous observation of a DNA-binding protein displacement by the concerted action of multiple Dda helicases aligned along ssDNA (39).

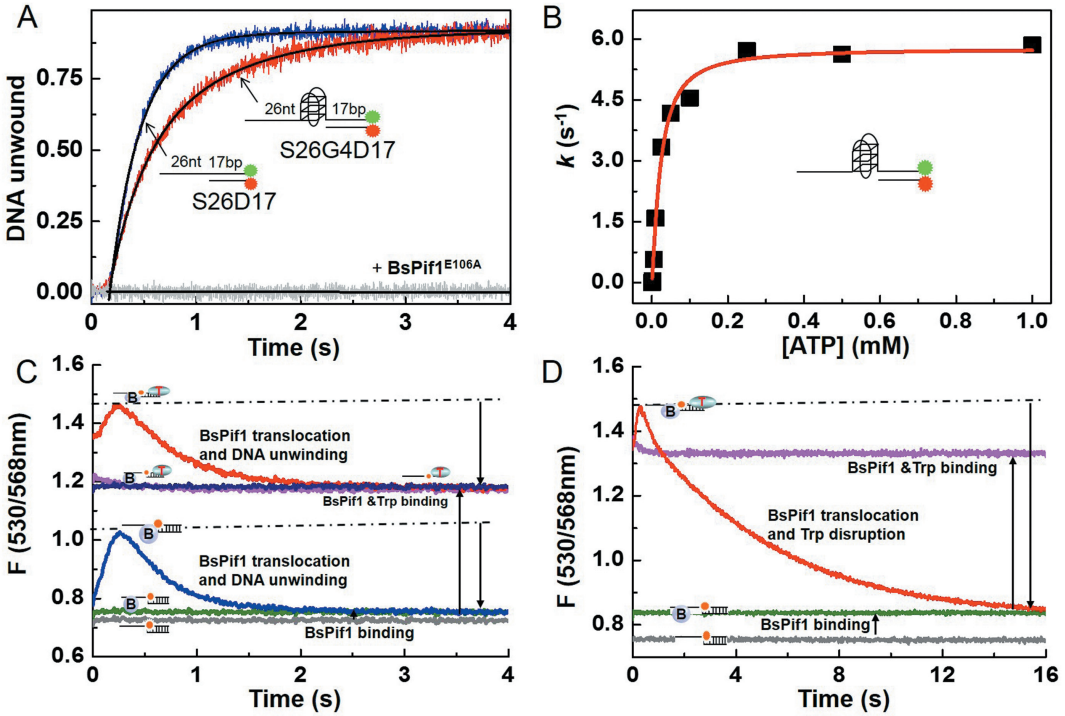

Figure 5. BsPif1 unwinds G4 structures and disrupts nucleoprotein complexes. (**A**) BsPif1-dependent unwinding of a partial duplex DNA containing or not a G4 motif inserted at the ss/dsDNA junction. Protein and DNA concentrations were 100 and 4 nM, respectively. (**B**) G4 unwinding kinetic rate constant as a function of ATP concentration. The curve was fitted according to a hyperbolic saturation function, giving $K_{d,ATP} = 22.8 \pm 2.6$ μM. (**C**) Time courses of BsPif1 translocation and DNA unwinding in the presence of 5 μM protein trap (T_{56}). Protein (BsPif1 or *trp* repressor) and DNA (Trp-D16-HF) concentrations were 10 and 20 nM, respectively, and ATP concentration was 1 mM. The fluorescence emission of hexachlorofluorescein was recorded using excitation and emission wavelengths at 530 and 568 nm, respectively. (**D**) BsPif1-dependent disruption of the *trp* repressor from DNA in the absence of protein trap. Except for protein trap, the concentrations are similar to those used in panel C. The plots in panels A, C and D are representative of three independent experiments.

DISCUSSION

In this study, we characterized the biochemical properties of the purified recombinant Pif1 helicase from *Bacteroides sp. 3_1_23* in terms of hydrodynamics and enzymatic properties. We found that BsPif1 functions as a monomer, and binds to a broad range of DNA substrates with, however, preferences toward structured DNAs in terms of affinity. Among the different DNA substrates, BsPif1 efficiently unwinds various structured DNAs including partial duplex DNA, fork-like substrates, D-loop and flap-like substrates. These observations indicate that BsPif1 helicase, like its eukaryotic homologues, may act at stalled DNA replication forks and enhance Okazaki fragment maturation. Thus BsPif1 helicases may have the potential ability to resolve many DNA substrate structures formed in the cell context at various stages of DNA metabolism including replication, transcription, repair and chromosome segregation.

Surprisingly, BsPif1 displays notable differences with ScPif1, but resembles human Pif1 in several qualitative aspects: (i) although the oligomeric state of human Pif1 is not yet determined, ScPif1 exists as a monomer in solution but becomes dimeric upon DNA-binding (20). From this point of view, DLS and gel filtration results show that BsPif1 is consistently monomeric even in the presence of DNA and/or ATP. The study of the relationship between the unwinding rate and ATP concentration further confirmed that BsPif1 primarily functions as a monomer during DNA unwinding. (ii) We found that BsPif1 can use indifferently all (deoxy)nucleotides as energy source for DNA unwinding while it was previously reported that ScPif1 uses preferentially ATP/dATP (6). (iii) ScPif1 unwinds forked duplex DNAs more efficiently than partial duplex (ss/ds) DNAs (24). This is in sharp contrast to BsPif1 which, like human Pif1, unwinds partial duplex DNAs more efficiently than forked duplex DNAs. Although a majority of helicases prefers a forked duplex over a ssDNA tail-containing duplex for unwinding, this is not a general property shared by all helicases. For example, the helicase core of *Sgs1* recombinant protein preferentially unwinds a 3′-ssDNA tail-containing duplex compared with a forked duplex DNA (40). The apparent differences in the substrate preference between ScPif1 and BsPif1 helicases may reflect an intrinsic structural property of the proteins. Taking into account the monomeric status of BsPif1 helicase as mentioned above, one could imagine that the forked DNA substrate enforces oligomerization (e.g. dimerization) of Pif1, with beneficial and detrimental effects on helicase activity of ScPif1 (20) and BsPif1, respectively. An alternative explanation that does not necessarily involve BsPif1 dimerization, could be related to a distribution of BsPif1 monomers on the two ssDNA tails of the fork substrate, productive (on the 5′-ssDNA tail) and not productive (on the 3′-ssDA tail), respectively, in terms of DNA unwinding. In this case, the

presence of the 3′-ssDNA tail in the forked DNA substrate could result in a sequestration of BsPif1 monomers and a decrease of the unwinding activity compared to the partial duplex (ss/ds) DNA. Further mechanistic studies regarding this property should be addressed. (iv) A previous study has shown that ScPif1 preferentially unwinds RNA/DNA hybrids over DNA/DNA duplexes (36). This phenomenon was interpreted as a physical basis for ScPif1-mediated telomerase disruption from telomere (36). Although some prokaryotic species possess linear chromosomes and telomeres (e.g. Streptomyces, Borrelia), most bacteria, including *Bacteroides sp. 3_1_23*, have circular genomes and thus no telomere. We found that BsPif1 was more potent for unwinding DNA/DNA than RNA/DNA substrates. This is in accordance with the absence of telomerase in *Bacteroides sp. 3_1_23*. However, although its RNA/DNA unwinding activity is relatively lower than DNA/DNA unwinding, BsPif1 still displays significant RNA/DNA unwinding activity, especially regarding the resolution of the R-loop structure. We believe that BsPif1 plays important roles in R-loop resolution for maintaining genome integrity since R-loop accumulation during transcription threatens genomic stability both in prokaryotic and eukaryotic organisms (35). (v) One of the most striking feature of ScPif1 helicases is that it binds strongly and unwinds more efficiently G4 DNA than the canonical double helix and other non-B form DNA secondary structures (12). However, based on both unwinding rate and reaction amplitude parameters, BsPif1 was not found to unwind G4 DNA more efficiently than a partial duplex DNA. Again, the property that BsPif1 unwinds G4 DNA as well as partial duplex substrates resembles that of human Pif1 which unwinds G4 DNA but with a lower efficiency compared with the partial duplex DNA (41). More interestingly, the ScPif1-mediated duplex DNA unwinding was greatly stimulated by the presence of a G4 motif (21) while BsPif1 did not display such a property. (vi) Finally, with regard to the ability to displace *trp* repressor from DNA, BsPif1 shares similar properties with ScPif1 and its closely related ScRrm3 helicase member. ScPif1 has been shown to disrupt telomerase from telomere and the second Pif1 family helicase ScRrm3 is thought to disrupt stable, non-nucleosomal protein–DNA complexes to avoid inhibition of the replication fork progression (10). BsPif1 and ScRrm3 sequences are homologous with 26.4% identity and 38.4% similarity. It is possible that BsPif1, like ScRrm3, possesses the ability to disrupt non-histone proteins from DNA. Our results based on the *trp* repressor system confirm that BsPif1 displays a strong activity of protein displacement. From the best of our knowledge, this is the first experimental demonstration that a Pif1 family helicase displaces non-nucleosomal protein *in vitro*. This activity may be reminiscent of the nucleoprotein disruption activity of ScRrm3 (42), which can remove RNA polymerase from the path of replication forks when replication and transcription complexes collide.

The above observation that BsPif1 enzymatically resembles more hPif1 than ScPif1 is somewhat surprising. One of the possibilities is that, until now, most of the studies relative to hPif1 have been performed with a truncated hPif1 helicase in which the N-terminal (pos. 1–205) and the C-terminal (pos. 621–641) sequences were deleted, leaving hPif1 helicase core domain (pos. 206–620). Thus, this hPif1 domain resembles the full-length BsPif1 which naturally lacks N- and C-terminal domains. Sequence alignment analysis shows that all essential structural motifs characterizing Pif1 helicases were well-conserved in BsPif1 and hPif1 helicase core without significant sequence deletion or insertion between the conserved motifs. Moreover, ScPif1 has an insertion of ≈80 amino acids between motifs IV and V which is almost absent in both BsPif1 and hPif1 proteins. This insertion may be responsible for the specific properties of ScPif1 and may explain why BsPif1 and ScPif1 display different properties. Unfortunately, deletion of this insertion sequence from ScPif1 resulted in the formation of inclusion bodies during protein expression, impeding further characterizations (data not shown). Quantitative and comparative analysis as well as kinetic parameter determination of the full length or/and truncated hPif1 and BsPif1 could provide more mechanistic comprehension about helicases of the Pif1 family. This comparison is currently under investigation in our laboratory.

In conclusion, our results show that BsPif1 resembles more human Pif1 protein than ScPif1 with regard to substrate specificity, helicase activity and mode of action. Although these comparisons are not based on experiments performed under strictly identical conditions, these comparisons of biochemical properties of Pif1 helicases may provide, at least qualitatively, biochemical basis to get deeper insight into the physiological functions of BsPif1 *in vivo* and will help to interpret future genetic study data obtained from prokaryotic model organisms encoding Pif1-like helicases.

SUPPLEMENTARY DATA

Supplementary Data are available at NAR Online.

ACKNOWLEDGEMENT

We thank Bio-Logic Company (France) for their special traveling to China for timely repairing our stopped-flow instruments.

FUNDING

National Natural Science Foundation of China [31370798, 11304252, 31301632]; 985 and 211 Projects from the Ministry of Education of China; LIA (in part). Chinese Universities Scientific Fund (QN2013036). Funding for open access charge: College of Life Sciences, Northwest A&F University.
Conflict of interest statement. None declared.

REFERENCES

1. Lohman,T.M., Tomko,E.J. and Wu,C.G. (2008) Non-hexameric DNA helicases and translocases: mechanisms and regulation. *Nat. Rev. Mol. Cell Biol.*, **9**, 391–401.
2. Matson,S.W., Bean,D.W. and George,J.W. (1994) DNA Helicases: enzymes with essential roles in all aspects of DNA metabolism. *Bioessays*, **16**, 13–22.
3. Chu,W.K. and Hickson,I.D. (2009) RecQ helicases: multifunctional genome caretakers. *Nat. Rev. Cancer*, **9**, 644–654.

4. Bessler,J.B., Torres,J.Z. and Zakian,V.A. (2001) The Pif1p subfamily of helicases: region-specific DNA helicases? *Trends Cell Biol.*, **11**, 60–65.
5. Chung,W.H. (2014) Topeep into Pif1 helicase: multifaceted all the way from genome stability to repair-associated DNA synthesis. *J. Microbiol.*, **52**, 89–98.
6. Lahaye,A., Leterme,S. and Foury,F. (1993) Pif1 DNA helicase from Saccharomyces Cerevisiae. Biochemical characterization of the enzyme. *J. Biol. Chem.*, **268**, 26155–26161.
7. Boule,J.B., Vega,L.R. and Zakian,V.A. (2005) The yeast Pif1p helicase removes telomerase from telomeric DNA. *Nature*, **438**, 57–61.
8. Paeschke,K., Capra,J.A. and Zakian,V.A. (2011) DNA replication through G-quadruplex motifs is promoted by the Saccharomyces cerevisiae Pif1 DNA helicase. *Cell*, **145**, 678–691.
9. Ivessa,A.S., Lenzmeier,B.A., Bessler,J.B., Goudsouzian,L.K., Schnakenberg,S.L. and Zakian,V.A. (2003) The Saccharomyces cerevisiae helicase Rrm3p facilitates replication past nonhistone protein-DNA complexes. *Mol. Cell*, **12**, 1525–1536.
10. Ivessa,A.S., Zhou,J.Q., Schulz,V.P., Monson,E.K. and Zakian,V.A. (2002) Saccharomyces Rrm3p, a 5′ to 3′ DNA helicase that promotes replication fork progression through telomeric and subtelomeric DNA. *Gene Dev.*, **16**, 1383–1396.
11. Kobayashi,T. (2003) The replication fork barrier site forms a unique structure with Fob1p and inhibits the replication fork. *Mol. Cell Biol.*, **23**, 9178–9188.
12. Paeschke,K., Bochman,M.L., Garcia,P.D., Cejka,P., Friedman,K.L., Kowalczykowski,S.C. and Zakian,V.A. (2013) Pif1 family helicases suppress genome instability at G-quadruplex motifs. *Nature*, **497**, 458–462.
13. Garg,P., Stith,C.M., Sabouri,N., Johansson,E. and Burgers,P.M. (2004) Idling by DNA polymerase delta maintains a ligatable nick during lagging-strand DNA replication. *Genes Dev.*, **18**, 2764–2773.
14. Pike,J.E., Henry,R.A., Burgers,P.M.J., Campbell,J.L. and Bambara,R.A. (2010) An alternative pathway for okazaki fragment processing resolution of fold-back flaps by Pif1 helicase. *J. Biol. Chem.*, **285**, 41712–41723.
15. Bochman,M.L., Judge,C.P. and Zakian,V.A. (2011) The Pif1 family in prokaryotes: what are our helicases doing in your bacteria? *Mol. Biol. Cell*, **22**, 1955–1959.
16. Czernik,P.J., Shin,D.S. and Hurlburt,B.K. (1994) Functional selection and characterization of DNA-binding sites for Trp repressor of Escherichia-Coli. *J. Biol. Chem.*, **269**, 27869–27875.
17. Xu,Y.N., Bazeille,N., Ding,X.Y., Lu,X.M., Wang,P.Y., Bugnard,E., Grondin,V., Dou,S.X. and Xi,X.G. (2012) Multimeric BLM is dissociated upon ATP hydrolysis and functions as monomers in resolving DNA structures. *Nucleic Acids Res.*, **40**, 9802–9814.
18. Zhang,X.D., Dou,S.X., Xie,P., Hu,J.S., Wang,P.Y. and Xi,X.G. (2006) Escherichia coli RecQ is a rapid, efficient, and monomeric helicase. *J. Biol. Chem.*, **281**, 12655–12663.
19. Lucius,A.L., Maluf,N.K., Fischer,C.J. and Lohman,T.M. (2003) General methods for analysis of sequential 'n-step' kinetic mechanisms: application to single turnover kinetics of helicase-catalyzed DNA unwinding. *Biophys. J.*, **85**, 2224–2239.
20. Barranco-Medina,S. and Galletto,R. (2010) DNA Binding Induces Dimerization of Saccharomyces cerevisiae Pif1. *Biochemistry*, **49**, 8445–8454.
21. Duan,X.L., Liu,N.N., Yang,Y.T., Li,H.H., Li,M., Dou,S.X. and Xi,X.G. (2015) G-quadruplexes significantly stimulate Pif1 helicase-catalyzed duplex DNA unwinding. *J. Biol. Chem.*, **290**, 7722–7735.
22. Gu,Y.Q., Masuda,Y. and Kamiya,K. (2008) Biochemical analysis of human PIF1 helicase and functions of its N-terminal domain. *Nucleic Acids Res.*, **36**, 6295–6308.
23. George,T., Wen,Q., Griffiths,R., Ganesh,A., Meuth,M. and Sanders,C.M. (2009) Human Pif1 helicase unwinds synthetic DNA structures resembling stalled DNA replication forks. *Nucleic Acids Res.*, **37**, 6491–6502.
24. Ramanagoudr-Bhojappa,R., Chib,S., Byrd,A.K., Aarattuthodiyil,S., Pandey,M., Patel,S.S. and Raney,K.D. (2013) Yeast Pif1 helicase exhibits a one-base-pair stepping mechanism for unwinding duplex DNA. *J. Biol. Chem.*, **288**, 16185–16195.
25. Ramanagoudr-Bhojappa,R., Byrd,A.K., Dahl,C. and Raney,K.D. (2014) Yeast Pif1 accelerates annealing of complementary DNA strands. *Biochemistry*, **53**, 7659–7669.
26. Harmon,F.G. and Kowalczykowski,S.C. (2001) Biochemical characterization of the DNA helicase activity of the Escherichia coli RecQ helicase. *J. Biol. Chem.*, **276**, 232–243.
27. Li,N., Henry,E., Guiot,E., Rigolet,P., Brochon,J.C., Xi,X.G. and Deprez,E. (2010) Multiple Escherichia coli RecQ helicase monomers cooperate to unwind long DNA substrates: a fluorescence cross-correlation spectroscopy study. *J. Biol. Chem.*, **285**, 6922–6936.
28. Azzalin,C.M., Reichenbach,P., Khoriauli,L., Giulotto,E. and Lingner,J. (2007) Telomeric repeat-containing RNA and RNA surveillance factors at mammalian chromosome ends. *Science*, **318**, 798–801.
29. Stith,C.M., Sterling,J., Resnick,M.A., Gordenin,D.A. and Burgers,P.M. (2008) Flexibility of eukaryotic Okazaki fragment maturation through regulated strand displacement synthesis. *J. Biol. Chem.*, **283**, 34129–34140.
30. Rossi,M.L., Pike,J.E., Wang,W., Burgers,P.M.J., Campbell,J.L. and Bambara,R.A. (2008) Pif1 helicase directs eukaryotic Okazaki fragments toward the two-nuclease cleavage pathway for primer removal. *J. Biol. Chem.*, **283**, 27483–27493.
31. Pike,J.E., Burgers,P.M.J., Campbell,J.L. and Bambara,R.A. (2009) Pif1 helicase lengthens some Okazaki fragment flaps necessitating Dna2 nuclease/helicase action in the two-nuclease processing pathway. *J. Biol. Chem.*, **284**, 25170–25180.
32. Saini,N., Ramakrishnan,S., Elango,R., Ayyar,S., Zhang,Y., Deem,A., Ira,G., Haber,J.E., Lobachev,K.S. and Malkova,A. (2013) Migrating bubble during break-induced replication drives conservative DNA synthesis. *Nature*, **502**, 389–392.
33. Wilson,M.A., Kwon,Y., Xu,Y., Chung,W.H., Chi,P., Niu,H., Mayle,R., Chen,X., Malkova,A., Sung,P. *et al.* (2013) Pif1 helicase and Poldelta promote recombination-coupled DNA synthesis via bubble migration. *Nature*, **502**, 393–396.
34. Brown,G.G., Gadaleta,G., Pepe,G., Saccone,C. and Sbisa,E. (1986) Structural conservation and variation in the D-loop-containing region of vertebrate mitochondrial DNA. *J. Mol. Biol.*, **192**, 503–511.
35. Aguilera,A. and Garcia-Muse,T. (2012) R loops: from transcription byproducts to threats to genome stability. *Mol. Cell*, **46**, 115–124.
36. Boule,J.B. and Zakian,V.A. (2007) The yeast Pif1p DNA helicase preferentially unwinds RNA DNA substrates. *Nucleic Acids Res.*, **35**, 5809–5818.
37. Byrd,A.K. and Raney,K.D. (2006) Displacement of a DNA binding protein by Dda helicase. *Nucleic Acids Res.*, **34**, 3020–3029.
38. Liu,Y.C. and Matthews,K.S. (1993) Dependence of Trp repressor-operator affinity, stoichiometry, and apparent cooperativity on DNA-sequence and size. *J. Biol. Chem.*, **268**, 23239–23249.
39. Byrd,A.K. and Raney,K.D. (2004) Protein displacement by an assembly of helicase molecules aligned along single-stranded DNA. *Nat. Struct. Mol. Biol.*, **11**, 531–538.
40. Bennett,R.J., Keck,J.L. and Wang,J.C. (1999) Binding specificity determines polarity of DNA unwinding by the Sgs1 protein of S-cerevisiae. *J. Mol. Biol.*, **289**, 235–248.
41. Sanders,C.M. (2010) Human Pif1 helicase is a G-quadruplex DNA-binding protein with G-quadruplex DNA-unwinding activity. *Biochem. J.*, **430**, 119–128.
42. Azvolinsky,A., Giresi,P.G., Lieb,J.D. and Zakian,V.A. (2009) Highly transcribed RNA polymerase II genes are impediments to replication fork progression in Saccharomyces cerevisiae. *Mol. Cell*, **34**, 722–734.